Journal of Maps

ISSN: (Print) (Online) Journal homepage: https://www.tandfonline.com/loi/tjom20

Echo-character distribution in the Cantabrian Margin and the Biscay Abyssal Plain

Adolfo Maestro, Alba Gallastegui, Mercedes Moreta, Estefanía Llave, Fernando Bohoyo, María Druet, Javier Navas, Sandra Mink, Fernando Fernández-Sáez, Manuel Catalán, María Gómez-Ballesteros, Alfonso Muñoz-Martín & José Luis Granja-Bruña

To cite this article: Adolfo Maestro, Alba Gallastegui, Mercedes Moreta, Estefanía Llave, Fernando Bohoyo, María Druet, Javier Navas, Sandra Mink, Fernando Fernández-Sáez, Manuel Catalán, María Gómez-Ballesteros, Alfonso Muñoz-Martín & José Luis Granja-Bruña (2021) Echo-character distribution in the Cantabrian Margin and the Biscay Abyssal Plain, Journal of Maps, 17:2, 533-542, DOI: 10.1080/17445647.2021.1973917

To link to this article: https://doi.org/10.1080/17445647.2021.1973917

JOURNAL OF MAPS
2021, VOL. 17, NO. 2, 533–542
https://doi.org/10.1080/17445647.2021.1973917

Taylor & Francis
Taylor & Francis Group

Science

Echo-character distribution in the Cantabrian Margin and the Biscay Abyssal Plain

Adolfo Maestro [a], Alba Gallastegui[a], Mercedes Moreta[a], Estefanía Llave[a], Fernando Bohoyo [a], María Druet [a], Javier Navas[a], Sandra Mink[a], Fernando Fernández-Sáez[a], Manuel Catalán [b], María Gómez-Ballesteros[c], Alfonso Muñoz-Martín[d] and José Luis Granja-Bruña [d]

[a]Instituto Geológico y Minero de España, Madrid, Spain; [b]Real Instituto y Observatorio de la Armada, Cádiz, Spain; [c]Instituto Español de Oceanografía, Madrid, Spain; [d]Departamento de Geodinámica, Estratigrafía y Paleontología, Universidad Complutense de Madrid, Madrid, Spain

ABSTRACT

In 2003, 2006–2009, 2014 and 2015, seven oceanographic cruises were carried out on board the Spanish R/V Hespérides in the Cantabrian Margin and the adjacent abyssal plains, covering an area of 219,124 km^2. Based on the combined analysis and interpretation of the bathymetric and reflectivity data obtained with multibeam echo sounders (SIMRAD EM12, EM120 and EM1002), and ultra-high-resolution reflection seismic records acquired with the SIMRAD TOPAS PS18 parametric sounder, the mapping of the acoustic facies or echo-character at a scale of 1:1,200,000 has been carried out. Thirty types of echoes have been differentiated and gather into four main groups: Distinct, Irregular, Hyperbolic and Undulated. The echo-character depends on the acoustic response of the shallow sediment and the seabed morphology. Therefore, its analysis and characterization are basic for understanding recent and present-day sedimentary processes.

ARTICLE HISTORY
Received 10 May 2021
Accepted 23 August 2021

KEYWORDS
Bathymetry; Cantabrian Margin; echo-character; parametric echo-sounder seismic profiles; reflectivity

1. Introduction

The intrinsic capability of each sediment type to differentially absorb and scatter sound waves allows the geophysical systems to differentiate types and architecture of sedimentary deposits. The processes behind sediment deposition are strongly influenced by factors such as the geological setting, sediment supply, oceanographic and paleoclimate conditions and sea level fluctuations (Davis et al., 2002). From recognizing the importance of the physical and acoustic properties of marine sediments, many studies used echo-characters to understand recent sedimentary processes in ocean basins. Since the 1950s, acoustic facies analysis based on seismic records (e.g. 3.5 kHz, pinger, 12 kHz, TOPAS or Parametric Sounder) has been a relevant technique for the study of sediment type as well as sedimentary processes in deep marine environments. Former studies based on the analysis of seabed reflectivity were carried out by Heezen et al. (1959) and Hollister and Heezen (1972). J. E. Damuth established by first time the acoustic classification response in deep-sea environments based on the analysis of seabed reflectivity (Damuth, 1975, 1978, 1980; Damuth et al., 1983, 1988; Damuth & Hayes, 1977). Numerous studies have ever since confirmed the effectiveness of using the echo-character as an indirect method for the characterization of sedimentary processes (e.g. Hernández-Molina et al., 2008; Llave et al., 2018; Maestro et al., 2018; Pratson & Laine, 1989; among others).

This work presents for the first time a mapping of the echo-character of the Cantabrian Margin and the adjacent abyssal plains at a scale of 1:1,200,000 prepared by the Spanish Geological and Mining Institute in collaboration with the Hydrographic Institute of the Spanish Navy and the Spanish Royal Navy Observatory, the Spanish Institute of Oceanography and the Complutense University of Madrid. This mapping is a product of the 'Scientific Research Project of the Spanish Exclusive Economic Zone' led by the Spanish Ministry of Defence.

2. Geologic and oceanographic settings

The present-day configuration of the northern margin of Iberia is due to its tectonic evolution since the Mesozoic (Figure 1). There were several episodes of continental crustal transpression and extension, between the Valanginian-Barremian and the Aptian, related to the opening of the Atlantic Ocean, with the Bay of Biscay being a branch of the main rift (e.g. Ziegler, 1989). This process involved a counter-clockwise rotation of the Iberian Plate related to the Eurasian Plate (e.g. Olivet et al., 1984). Extensional tectonics resulted in the development of large normal faults and tilted blocks of approximately WNW-ESE

CONTACT Adolfo Maestro a.maestro@igme.es Instituto Geológico y Minero de España, C/ La Calera, 1, Tres Cantos, Madrid 28760, Spain

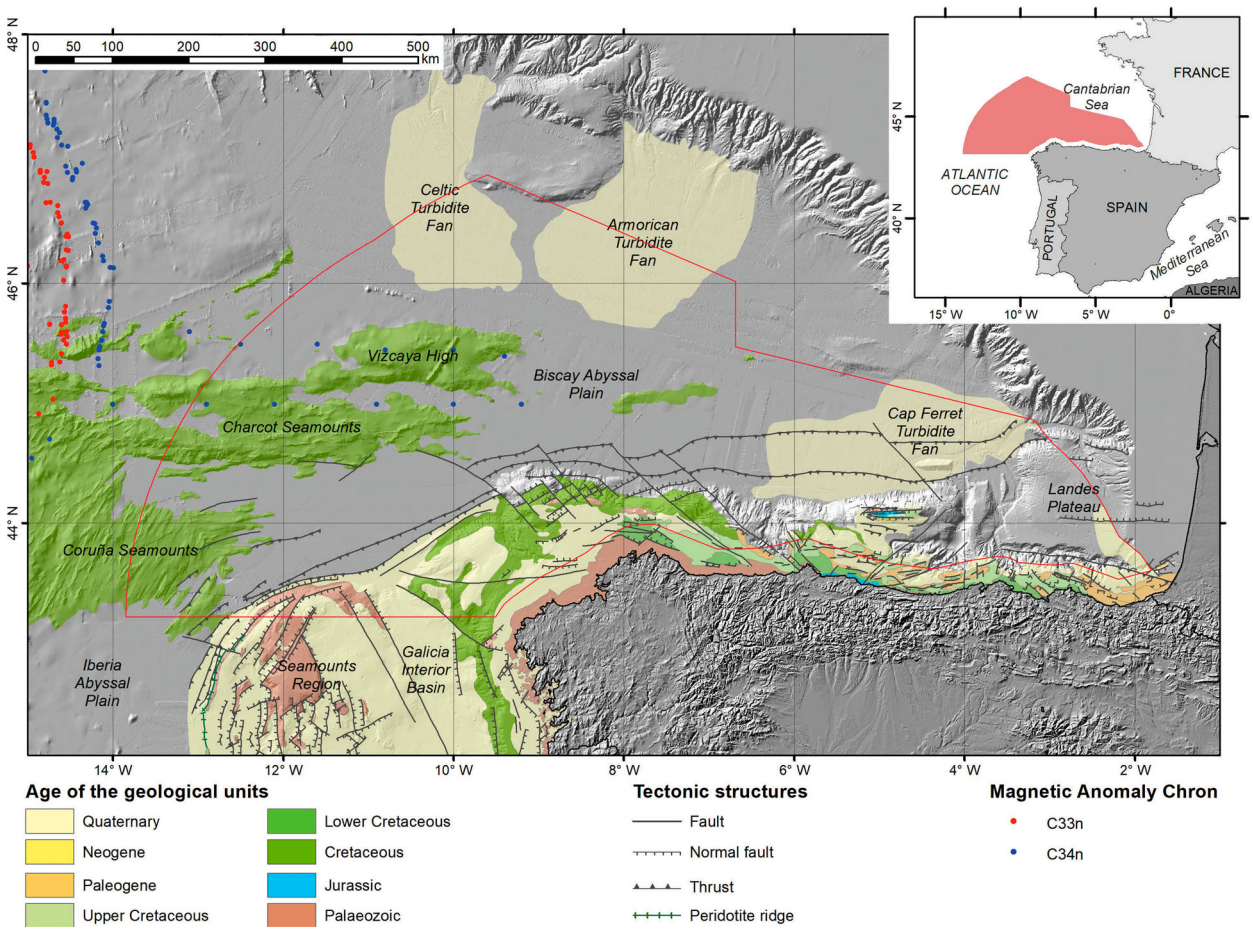

Figure 1. Sketched geological and tectonic setting of the northern Iberian continental margin and adjacent abyssal domains modified from Rodríguez-Fernández et al. (2014). Magnetic anomaly picks from Seton et al. (2014). Background DMT from EMODnet (https://www.emodnet-bathymetry.eu/).

to E-W direction on the northern Iberian margin, and NE-SW on the north-western Iberian margin, at the transition to the western margin. In the last phase of the rifting process (Aptian), the continental crust was hyperextended and the lithospheric mantle was exhumed. After the extensional stage, in the Albian, the generation of oceanic crust and partial westward drift began in the Bay of Biscay, ending in the Santonian (Tugend et al., 2015 and references therein) (Figure 1). Along the northern sector of Iberia, this continental rifting process occurred diachronically, in two large segments: the Bay of Biscay-Parentis Basin, and the Pyrenees-Basque-Cantabrian Basin. The development of these rift segments was controlled by the tectonic inheritance of previous structures (e.g. Druet et al., 2018; Tugend et al., 2015). The different basins located in these segments were separated by faults and transfer zones with N-S to NNE-SSW direction (e.g. Druet et al., 2018; Tugend et al., 2015). In the Upper Cenomanian and until at least the Oligocene, the northward displacement of the African Plate causes the collision of the Iberian and Eurasian plates, leading to the formation of the Pyrenean orogen and the partial tectonic inversion of the north Iberian margin (e.g. Olivet et al., 1984; Tugend et al., 2015) (Figure 1). From the Miocene to the present-day, tectonic events of lesser intensity have taken place, predominantly in an NW-SE to WNW-ESE shortening direction, under a transtensional regime (e.g. Herraiz et al., 2000). These tectonic processes have fundamentally controlled the recent seafloor morphology with the formation of extensive marginal platforms, submarine banks and canyons and pockmark and pockform morphologies on the continental slope and seamounts on the abyssal plain (Iglesias et al., 2010; Jané et al., 2010; Llave et al., 2018) (Figure 1). Similarly, the sedimentary processes taking place since the Miocene have also controlled the present-day morphological features of the Cantabrian Margin and Biscay Abyssal Plain. These processes can be summarized in: (a) the development of: turbiditic systems, characterized by the presence of a complex abyssal or mesooceanic channel patterns, which drain sedimentary inputs coming from the Celtic, Armorican and Cap Ferret turbidity fans (e.g. Ercilla et al., 2008; Llave et al., 2018); (b) sedimentary deposits and erosional features linked to along-slope processes related to deep contour currents (Ercilla et al., 2008; Hernández-Molina et al., 2008; Llave et al., 2018); and (c) deposits related to gravity-driven processes located

on the flanks of the submarine highs on the continental slope and seamounts in the abyssal plain (Ercilla et al., 2008).

Most of the water masses circulating in the northwest and north of the Iberian Peninsula have their origin in the North Atlantic Current or are the result of the interaction between this and the Mediterranean Current (e.g. Pollard et al., 1996) (Figure 2). In the Cantabrian Sea, there are five main water masses located at different depths and with different thermohaline properties (Friocourt et al., 2007) (Figure 2). The shallowest body of water comprises the Portugal Current (PC), which flows southward while the Portugal Coastal Current (PCC) flows towards the north (Fiúza et al., 1998; Varela et al., 2005). The ENACW of subtropical origin (ENACWst) moves north and extends down to water depths of 600 m (Fiúza et al., 1998) and a component of ENACW of subpolar (ENACWsp) origin moves south from about 300 to 400 m of depth (Fiúza et al., 1998). From a depth of 600 m, the Mediterranean Outflow Water (MOW) extends to 1500 m (e.g. González-Pola, 2006). The MOW splits into two branches as it approaches the western sector of the Galicia Margin (Iorga & Lozier, 1999). One of the branches runs northwards across the Galician Interior Basin and then turns eastwards along the Cantabrian continental slope (González-Pola, 2006; Iorga & Lozier, 1999). The other branch runs around the western flank of the Galicia Bank and then continues northwards (González-Pola, 2006). Below the MOW is the Labrador Sea Water (LSW), which extends from 1500 m to 2500 m of

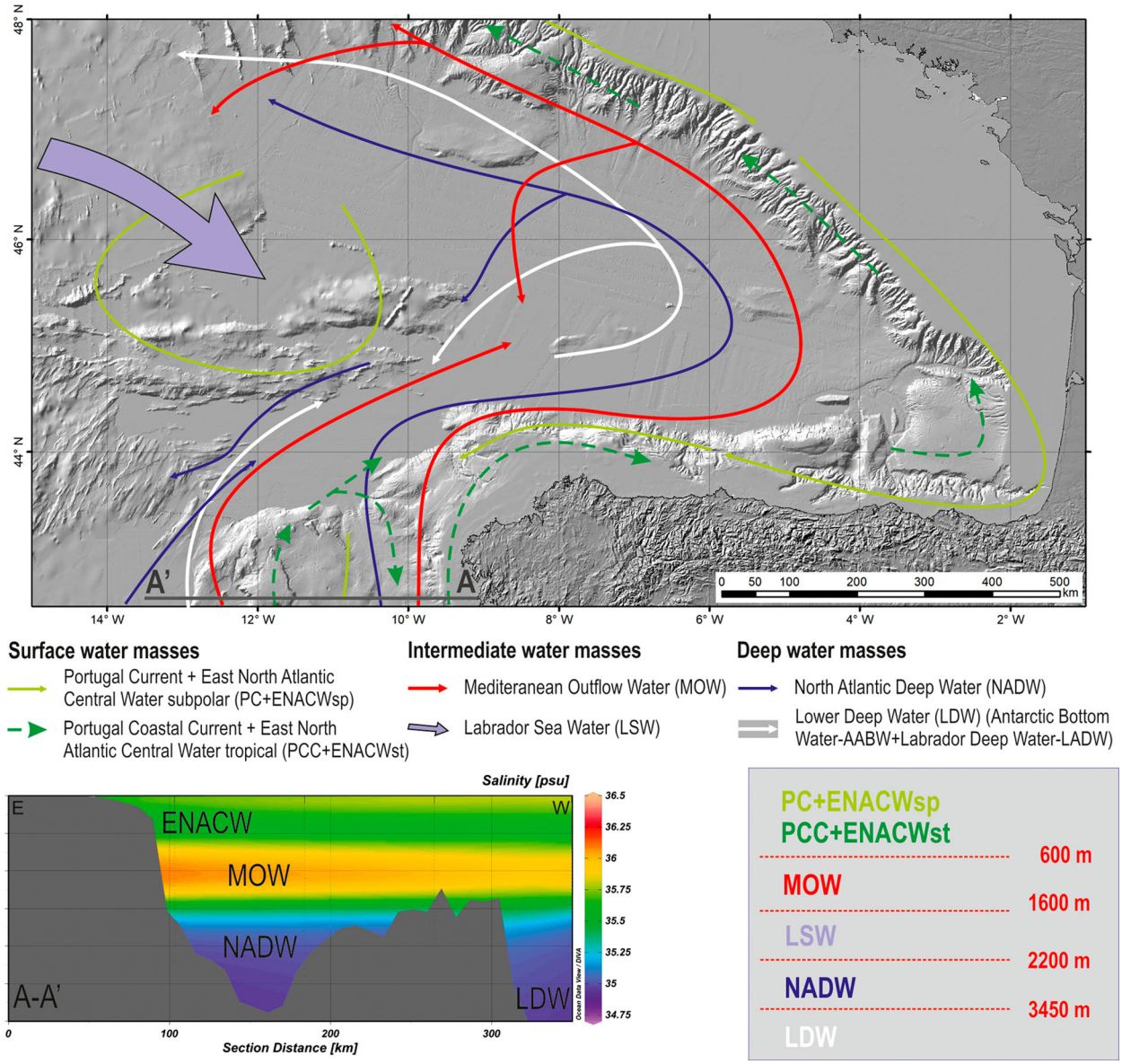

Figure 2. Superficial-, intermediate- and deep-water masses compilation around of the Galicia and Cantabrian continental margins and adjacent abyssal plains (modified from Hernández-Molina et al., 2008). Water masses: PC: Portugal Current; PCC: Portugal Coastal Current; ENACW: Eastern North Atlantic Central Water (with subpolar, ENACWsp, and subtropical, ENECWst, origin); MOW: Mediterranean Outflow Water; LSW: Labrador Sea Water; NADW: North Atlantic Deep Water; and LDW: Lower Deep Water. Background DMT from EMODnet (https://www.emodnet-bathymetry.eu/).

depth (González-Pola, 2006). In the Bay of Biscay, the LSW penetrates from the northwest (Paillet et al., 1998) and is characterized by an anticyclonic gyre. Between 2500 and 3000 m of depth is located the North Atlantic Deep Water (NADW) (e.g. González-Pola, 2006; McCartney, 1992; McCave et al., 2001). Below the NADW is the Lowered Deep Water (LDW), which is the result of mixing between the Antarctic Bottom Water (AABW) and the Labrador Deep Water (LADW) (e.g. McCartney, 1992; McCave et al., 2001). Internal waves and tides have also been described along the continental slope of the Bay of Biscay, due to the combination of the stratification of the water masses, their interaction with the irregularities of the seabed and the strong barotropic tidal currents generated by the tidal currents (e.g. Pingree & Le Cann, 1990; Zhang et al., 2016).

3. Acquisition and data analysis

The Kongsberg EM12 and EM120 multibeam echo sounders are designed to operate in deep water up to 11,000 m of depth, complying with the International Hydrographic Organisation (IHO) S-44 Standards for Hydrographic Surveys. The working central frequency was 13 kHz, and they have a maximum beamwidth of 120° and 150°, respectively, and use up to 191 beams, giving an average seabed coverage of about 3.5 times the depth. The Kongsberg EM1002 is used for high-resolution bathymetric surveys in shallow waters from 3 to 600 m of depth. The working central frequency was 95 kHz, and it has a maximum beamwidth of 150°. The accuracy of the sounder is also in accordance with IHO standards for high-resolution bathymetry. The maximum horizontal coverage is approximately 1000 m, although it depends on depth, varying from 5.5 to 7 times the depth at depths of 150 m. The Kongsberg EM12 and EM120 multibeam echo sounders can obtain sonography of the seafloor using their transmit array as the receiver. The multibeam sounder emits a high-frequency acoustic pulse through two channels, one on each side of the transducer and perpendicular to the ship's path, and then collects the reflected energy in a scattered manner (reflectivity or backscatter). Reflectivity is a function of the relief and texture of the seabed, but also depends on the frequency and incidence angle of the acoustic pulse. The acoustic pulse velocity in the water column depends on the local oceanographic conditions, such as temperature, salinity and density, so the use of conductivity-temperature-depth profilers or disposable bathythermographs (XBT) is necessary for the correct calculation of depth. During the seven oceanographic campaigns carried out, 70 XBTs have been used to obtain the data used for the mapping of the echo-character (Figure 3).

The SIMRAD TOPAS PS18 (Topographic Parametric Sonar) is an ultra-high-resolution seismic reflection system. The TOPAS system emits pulses at a primary frequency of 18 kHz, up to 30 kW of power. This system is based on the so-called 'parametric effect', which is the generation of relative low-frequency acoustic waves through the non-linear interaction, in the first metres of the water column, of two high-frequency sound beams. The resulting secondary frequency used by the sounder has a

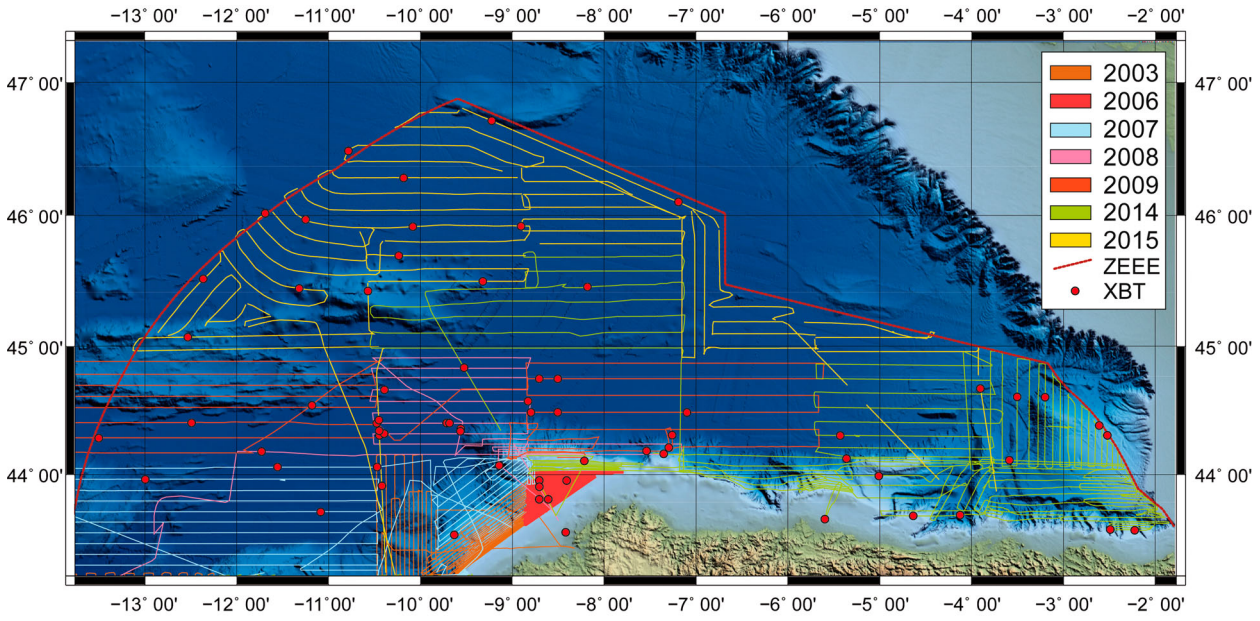

Figure 3. TOPAS PS18 parametric and multibeam echosounders (SIMRAD EM12, EM120 and EM1002) tracks carried out in the Cantabrian Continental Margin and adjacent abyssal plains during the 'Spanish Exclusive Economic Zone' oceanographic cruises in 2003, 2006–2009, 2014 and 2015. Moreover, the figure shows the position of the disposable bathythermographs (XBT) used. Background DMT from EMODnet (https://www.emodnet-bathymetry.eu/).

bandwidth frequency between 0.5 and 4.0 kHz. The advantage of the TOPAS system over conventional sub-bottom profiler systems (e.g. Chirp and 3.5-kHz) is that the secondary seismic pulse it uses, with a narrower and much more stable acoustic beam, allows higher resolution (tens of cm) and better penetration (90–100 ms TWTT) below the seafloor.

The data analysis was carried out in two phases: (1) echo-character classification based on ultra-high-resolution seismic reflection records acquired with the SIMRAD TOPAS PS18 parametric sounder; and (2) echo-characters mapping based on the high-resolution bathymetric and reflectivity data obtained with the Kongsberg EM12 (until 2004), EM120 (since 2005) and EM1002 (in 2006) multibeam echo sounders. A total of 596 high-resolution seismic profiles with a total length of 38,434 km, from seven oceanographic cruises carried out on board the R/V Hespérides during 2003, 2006, 2007, 2008, 2009, 2014 and 2015, have been analysed and interpreted. The mapped area covers an area of 219,124 km^2 (Figure 3).

4. Echo-character map elaboration processes

The echo-character map of the Cantabrian Margin has been produced at 1:1,200,000 scale (see Main Map). The geographical coordinate system used in the layout is Universal Transverse Mercator projection. The echo-character information has been incorporated into the map on a digital terrain model in order to easily visualize the distribution of echoes in relation to the seabed morphology. For this purpose, acoustic information on the seabed and sub-seabed and bathymetric information have been treated separately and thereafter integrated.

In order to carry out the echo-character mapping, the different acoustic facies were first defined and classified on the basis of ultra-high-resolution seismic profiles. Subsequently, their spatial distribution has been established by interpolating the different echoes defined in the seismic lines based on the morphology and reflectivity of the seabed (Figure 4). The mapping of polygons and topology analysis was carried out in ArcGIS v.10.6.

The Digital Terrain Model (DTM) was produced from an xyz file in ASCII format containing the bathymetry of the mapped area, combined with bathymetric information from the European Marine Observation and Data Network (EMODnet) to complete the marine areas where information of the SEEZ project was missing, and with EU-DEM v1.1 data from the Copernicus satellite network for the terrestrial areas. The processing was carried out with the FME 2019 application to generate a DTM with an X and Y regular resolution of 50 m in UTM-WGS84 projection and 0.000615° in WGS84 geographic coordinate system. The DTM was post-processed by identifying possible errors causing both unwanted depressions and peaks in the relief and removing them using a sink-filling algorithm. At the same time, the overlap zones between the different bathymetries were smoothed in those areas that presented problems. Finally, a low-pass filter was applied to remove the high-frequency noise. The shading model was generated from the DTM using multidirectional shading combined with a slope map to achieve a more natural result (see Main Map). This procedure allows to highlight morphologies that otherwise, using a single angle, may remain hide in shadow or direct light areas.

In the final layout of the map, other information layers were generated in addition to the mapping of the spatial distribution of the defined echo types and the digital terrain model. Among them, the bathymetry contour line layer was edited to generate depth information labelling following the direction of the contour line, and labels were added to identify reliefs and singular entities, both in the offshore and onshore zones (see Main Map). The appropriate colour palette and transparency were also chosen to allow the seabed shading to be seen and to make the map as clear and visually aesthetic as possible.

5. Echo-character classification

A specific classification has been developed for the study area using the methodology and based on the classifications proposed by Damuth (1975, 1978, 1980), Damuth and Hayes (1977) and Pratson and Laine (1989). Thirty types of echoes have been differentiated into four main classes (Figure 5): (1) Distinct echo, (2) Irregular echo, (3) Hyperbolic echo, and (4) Undulated echo.

5.1. Type 1: distinct echoes

This echo-type is characterized by distinct and uniform bottom echoes. It occupies a surface of about 125,100 km^2. Into this echo-type, 14 echo-subtypes have been differentiated in the study area, on the basis of sub-bottom acoustic facies, from A to N (Figure 5). They are located in the continental shelf and slope, and in the abyssal plain.

5.1.1. Subtype 1A

It is characterized by the absence of sub-bottom reflectors underneath a distinct continuous bottom echoes. This subtype shows an extension of 4058 km^2.

5.1.2. Subtype 1B

It is characterized by parallel and stratified sub-bottom reflectors underneath a distinct continuous bottom echoes. This subtype shows the largest extension of the study area, with a surface of 49,690 km^2.

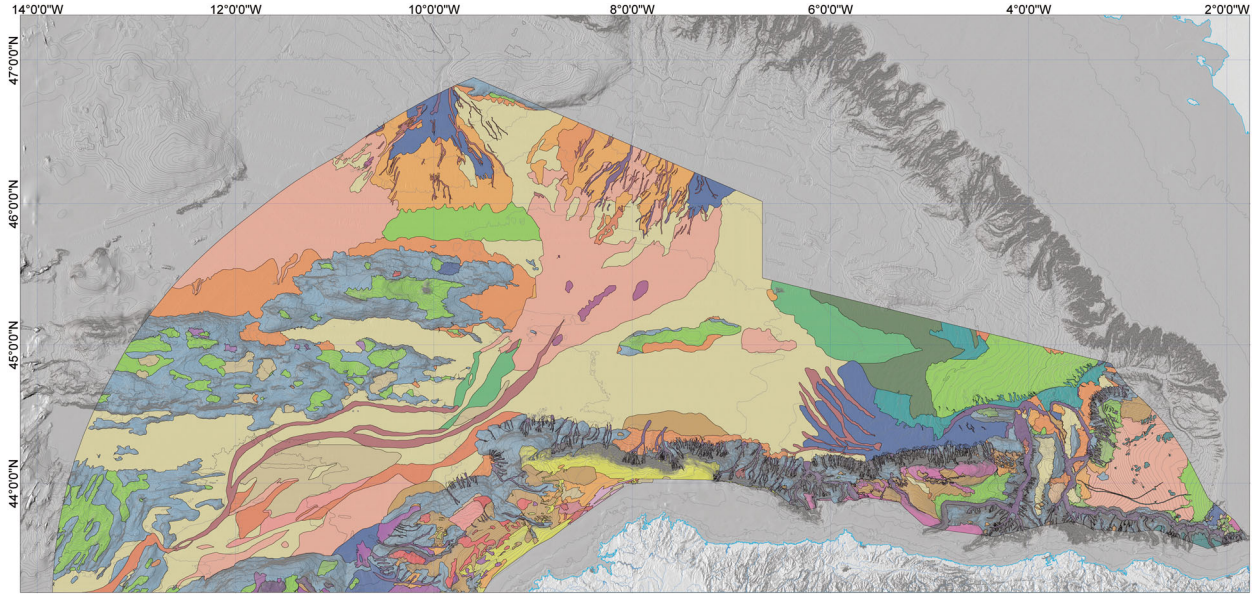

Figure 4. Echo-character map of the Cantabrian Continental Margin and adjacent abyssal plains showing the location and distribution of the different echo-subtypes identified on a shaded digital elevation model of the seabed. The echo-character colour legend is shown in Figure 5.

5.1.3. Subtype 1A

It is characterized by the absence of sub-bottom reflectors underneath a distinct continuous bottom echoes. This subtype shows an extension of 4058 km^2.

5.1.4. Subtype 1C

It is characterized by truncate sub-bottom reflectors underneath a distinct continuous bottom echoes. This subtype shows an extension of 9070 km^2.

5.1.5. Subtype 1D

It is characterized by a distinct and uniform bottom echo and sub-bottom acoustic blanking with stratified reflectors in the base. This subtype shows an extension of about 5400 km^2.

5.1.6. Subtype 1E

It is characterized by a distinct and uniform bottom echo and sub-bottom prograding reflectors. This subtype shows an extension of about 6630 km^2.

5.1.7. Subtype 1F

It is characterized by a distinct and uniform bottom echo and sub-bottom acoustic blanking with a distinct reflector in the base. This subtype shows an extension of 10,150 km^2.

5.1.8. Subtype 1G

It is characterized by a distinct and uniform bottom echo and sub-bottom stratified reflectors with acoustic blanking in the base. This subtype covers an area of approximately 230 km^2.

5.1.9. Subtype 1H

It is characterized by a distinct and uniform bottom echo and sub-bottom alternation of high reflective parallel reflectors to bottom and acoustic blanking levels. It has an extension of 29,030 km^2.

5.1.10. Subtype 1I

It is characterized by a distinct and uniform bottom echo and sub-bottom alternation of prograding and continuous reflectors and acoustic blanking levels. It occupies a total area of approximately 1310 km^2.

5.1.11. Subtype 1J

It is characterized by a distinct and uniform bottom echo and sub-bottom acoustic blanking with alternation of high reflective reflectors and acoustic blanking levels in the base. It has an extension of 3012 km^2.

5.1.12. Subtype 1K

It is characterized by a distinct and uniform bottom echo and sub-bottom oblique reflectors. This echo covers a surface of 114 km^2.

5.1.13. Subtype 1L

It is characterized by a distinct and uniform bottom echo and sub-bottom high reflective undulate, disrupted reflectors, parallel to each other but not to the bottom, with vertical transparent zones. This echo covers an area of 137 km^2.

5.1.14. Subtype 1M

It is characterized by a distinct and uniform bottom echo and sub-bottom high reflective undulate, truncate and parallel reflectors. It has an extension of 856 km^2.

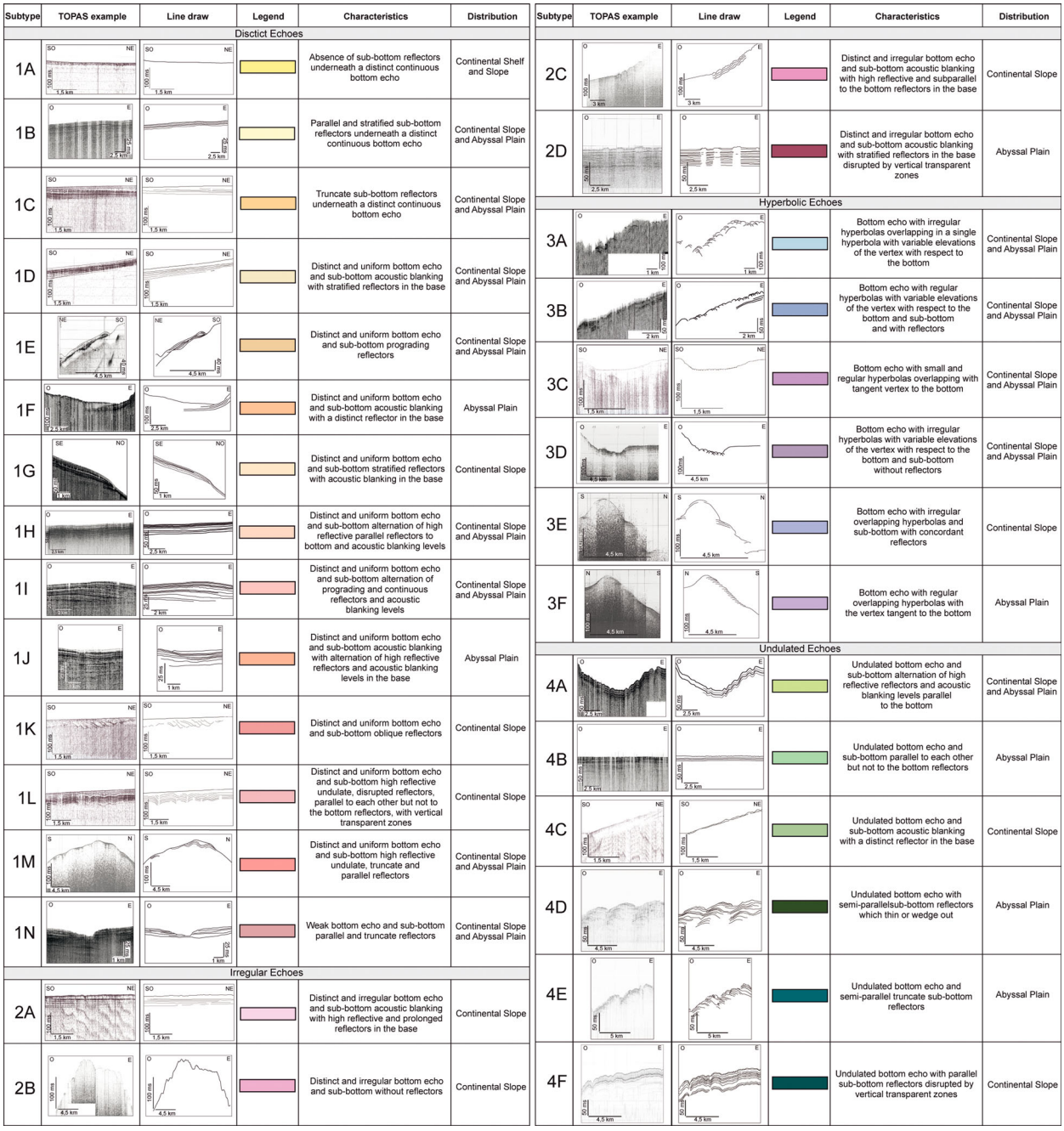

Figure 5. Echo-character types and subtypes classification established for the Cantabrian Continental Margin and adjacent abyssal plains map.

5.1.15. Subtype 1N

It is characterized by a weak bottom echo and sub-bottom parallel and truncate reflectors. This echo occupies an area of 5411 km^2.

5.2. Type 2: irregular echoes

This echo-type comprises distinct and irregular bottom echoes. Into this echo-type, four echo-subtypes have been differentiated in the study area, from A to D (Figure 5), occupying a surface of 2125 km^2. They are located in the continental slope and the abyssal plain.

5.2.1. Subtype 2A

It is characterized by a distinct and irregular bottom echo and sub-bottom acoustic blanking with high reflective and prolonged reflectors in the base. It covers an area of 185 km^2.

5.2.2. Subtype 2B

It is characterized by a distinct and irregular bottom echo and sub-bottom without reflectors. It presents an extension of 1465 km^2 within the mapped area.

5.2.3. Subtype 2C

It is characterized by a distinct and irregular bottom echo and sub-bottom acoustic blanking with high

reflective and subparallel to the bottom reflectors in the base. It has an area of 57 km^2.

5.2.4. Subtype 2D

It is characterized by a distinct and irregular bottom echo and sub-bottom acoustic blanking with stratified reflectors in the base disrupted by vertical transparent zones. It has an area of 418 km^2.

5.3. Type 3: hyperbolic echoes

This echo-type comprises prolonged and hyperbolic bottom echoes. It occupies a surface of about 60,559 km^2. Into this echo-type, six echo-subtypes have been differentiated in the study area, from A to F, depending on the relationship between the hyperbolas vertex with respect to the seafloor or the sub-bottom reflectors (Figure 5). They are located in the continental slope and the abyssal plain.

5.3.1. Subtype 3A

It is characterized by a bottom echo with irregular hyperbolas overlapping in a single hyperbola with variable elevations of the vertex with respect to the bottom. The hyperbolas wavelength can oscillate between 70 and 400 m and the amplitude does not exceed 25 m. This echo covers an area of 43,963 km^2.

5.3.2. Subtype 3B

It is characterized by a bottom echo with regular hyperbolas with variable elevations of the vertex with respect to the bottom and sub-bottom and with reflectors. The hyperbolas' average wavelength is about 5.5 km and the amplitude is approximately 7.5 m. This echo occupies an area of 8229 km^2.

5.3.3. Subtype 3C

It is characterized by a bottom echo with small and regular hyperbolas overlapping with tangent vertex to the bottom. The hyperbolas' wavelength is about 6 m and the mean amplitude is about 50 cm. This echo presents a surface of 1003 km^2.

5.3.4. Subtype 3D

It is characterized by a bottom echo with irregular hyperbolas with variable elevations of the vertex with respect to the bottom and sub-bottom without reflectors. The hyperbolas' wavelength varies between 0.5 and 1 km, and the amplitude is approximately 10 m. It has an extension of 7213 km^2.

5.3.5. Subtype 3E

It is characterized by a bottom echo with irregular overlapping hyperbolas and sub-bottom with concordant reflectors. The hyperbolas' wavelength varies between 1 and 2.5 km, and the amplitude is about 9 m. It has an extension of about 3 km^2.

5.3.6. Subtype 3F

It is characterized by a bottom echo with regular overlapping hyperbolas with the vertex tangent to the bottom. The hyperbolas' wavelength is about 0.9 m and the amplitude not exceeding 3 m. It has an extension of approximately 1730 km^2.

5.4. Type 4: undulated echoes

This echo-type comprises irregular bottom echoes that appear to be almost hyperbolic echoes. It shows a wide variety of shapes and sizes. This type of echo covers an area of 29,241 km^2 in the mapped area. Into this echo-type, six echo-subtypes have been differentiated, from A to F (Figure 5). They are located in the continental slope and the abyssal plain.

5.4.1. Subtype 4A

It is characterized by an undulated bottom echo and sub-bottom alternation of high reflective reflectors and acoustic blanking levels parallel to the bottom. This echo occupies an area of 18,263 km^2.

5.4.2. Subtype 4B

It is characterized by an undulated bottom echo and sub-bottom parallel to each other but not to the bottom reflectors. This echo covers a surface of 4186 km^2.

5.4.3. Subtype 4C

It is characterized by undulated bottom echo and sub-bottom acoustic blanking with a distinct reflector in the base. This echo occupies an extension of about 4 km^2.

5.4.4. Subtype 4D

It is characterized by an undulated bottom echo with semi-parallel sub-bottom reflectors which thin or wedge out. This echo occupies an area of 3776 km^2.

5.4.5. Subtype 4E

It is characterized by an undulated bottom echo and semi-parallel truncate sub-bottom reflectors. This echo occupies an area of 2518 km^2.

5.4.6. Subtype 4F

It is characterized by an undulated bottom echo with parallel sub-bottom reflectors disrupted by vertical transparent zones. This echo occupies an area of 487 km^2.

6. Conclusions

This paper presents the 1:1,200,000 scale echo-character map of the Cantabrian Margin. The map is based on the interpretation of high-resolution seismic profiles from the SIMRAD TOPAS PS18 parametric echo sounder and their correlation with bathymetry

and reflectivity data from the SIMRAD EM12, EM120 and EM1002 multibeam echo sounders. Data were obtained during the oceanographic cruises carried out in 2003, 2006–2009, 2014 and 2015 on board the R/V Hespérides. This mapping has been carried out within the framework of the 'Scientific Research Programme of the Spanish Exclusive Economic Zone' by the Spanish Geological and Mining Institute.

The map depicts the location, distribution and extent of the identified acoustic facies on a shaded digital terrain model of the seabed. Thirty eco-types have been identified and grouped into four main echoes: Distinct, Irregular, Hyperbolic and Undulated. This map provides a valuable regional base for interpreting the recent and present-day sedimentary processes in the region.

Software

The processing of the multibeam data has been carried out by the Hydrographic Institute of the Spanish Navy, using the Teledyne CARIS HIPS & SIPS software package. Digital Terrain Model was performed with the FME 2019 software. The correlation between the superficial acoustic facies, the mapping of polygons and edition of topology was performed in ArcGIS v.10.6. This information was later imported into the Adobe Illustrator CS3 software, where the final design and layout work was done.

Acknowledgements

We are grateful to the captains and crews of the R/V Hespérides. This project is leaded by the Hydrographic Institute of the Spanish Navy and the Spanish Royal Navy Observatory. This map was funded by the Geological and Mining Institute of Spain. We are also grateful for the comments, corrections and suggestions to the reviewers Dr. Heike Apps and Dr. Luiz Souza, and the Associate Editor Dr. Claudio Riccomini, which improved the original manuscript.

Disclosure statement

No potential conflict of interest was reported by the author(s).

Funding

This work was supported by the Instituto Geológico y Minero de España and the Spanish project SCORE (CGL2016-80445-R, AEI/FEDER, UE).

Data availability statement

The bathymetric and reflectivity data and the ultra-high-resolution seismic profiles used to elaborate the echo-character map of the Cantabrian Margin have been obtained in the framework of the 'Scientific Research Project of the Spanish Exclusive Economic Zone' led by the Spanish Ministry of Defence and they are not open data. For their consultation, please contact the Hydrographic Institute of the Spanish Navy (https://armada.defensa.gob.es/ArmadaPortal/page/Portal/ArmadaEspannola/cienciaihm1/prefLang-en/) and the Spanish Royal Navy Observatory (https://armada.defensa.gob.es/ArmadaPortal/page/Portal/ArmadaEspannola/cienciaobservatorio/prefLang-en/).

ORCID

Adolfo Maestro http://orcid.org/0000-0002-7474-725X
Fernando Bohoyo http://orcid.org/0000-0002-1044-8816
María Druet http://orcid.org/0000-0002-0534-0018
Manuel Catalán http://orcid.org/0000-0001-9691-7101
José Luis Granja-Bruña http://orcid.org/0000-0001-8741-5388

References

Damuth, J. E. (1975). Echo character of the western equatorial Atlantic floor and its relationship to the dispersal and distribution of terrigenous sediments. *Marine Geology*, *18* (2), 17–45. https://doi.org/10.1016/0025-3227(75)90047-X

Damuth, J. E. (1978). Echo character of the Norwegian-Greenland Sea: Relationship to Quaternary sedimentation. *Marine Geology*, *28*(1-2), 1–36. https://doi.org/10.1016/0025-3227(78)90094-4

Damuth, J. E. (1980). Use of high-frequency (3.5–12 kHz) echograms in the study of near-bottom sedimentation processes in the deep-sea: A review. *Marine Geology*, *38* (1-3), 51–75. https://doi.org/10.1016/0025-3227(80)90051-1

Damuth, J. E., Flood, R. D., Kowsmann, R. O., Belderson, R. H., & Gorini, M. A. (1988). Anatomy and growth pattern of Amazon deep-sea fan as revealed by long-range side-scan sonar (GLORIA) and highresolution seismic studies. *Bulletin of the American Association of Petroleum Geologists*, *72*(8), 885–911.

Damuth, J. E., & Hayes, D. E. (1977). Echo character of the East Brazilian continental margin and its relationship to sedimentary processes. *Marine Geology*, *24*(2), 73–95. https://doi.org/10.1016/0025-3227(77)90002-0

Damuth, J. E., Kolla, V., Flood, R. D., Kowsmann, R. O., Monteiro, M. C., Gorini, M. A., Palma, J. J. C., & Belderson, R. H. (1983). Distributary channel meandering and bifurcation patterns on the Amazon deep-sea fan as revealed by long-range side-scan sonar (GLORIA). *Geology*, *11*(2), 94–98. https://doi.org/10.1130/0091-7613(1983)11<94:DCMABP>2.0.CO;2

Davis, A., Haynes, R., Bennell, J., & Huws, D. (2002). Surficial seabed sediment properties derived from seismic profiler responses. *Marine Geology*, *182*(1-2), 209–223. https://doi.org/10.1016/S0025-3227(01)00235-3

Druet, M., Muñoz-Martín, A., Granja-Bruña, J. L., Carbó-Gorosabel, A., Acosta, J., Llanes, P., & Ercilla, G. (2018). Crustal structure and continent-ocean boundary along the Galicia continental margin (NW Iberia): Insights from combined gravity and seismic interpretation. *Tectonics*, *37*(5), 1576–1604. https://doi.org/10.1029/2017TC004903

Ercilla, G., Casas, D., Estrada, F., Vázquez, J. T., Iglesias, J., García, M., Gómez, M., Acosta, J., Gallart, J., Maestro-González, A., & Marconi Team. (2008). Morphosedimentary features and recent depositional architectural model of the Cantabrian continental

margin. *Marine Geology*, *247*(1-2), 61–83. https://doi.org/10.1016/j.margeo.2007.08.007

Fiúza, A. F. G., Hamann, M., Ambar, I., Díaz del Río, G. D., González, N., & Cabanas, J. M. (1998). Water masses and their circulation off western Iberia during May 1993. *Deep Sea Research Part I: Oceanographic Research Papers*, *45*(7), 1127–1160. https://doi.org/10.1016/S0967-0637(98)00008-9

Friocourt, Y., Levier, B., Speich, S., Blanke, B., & Drijfhout, S. S. (2007). A regional numerical ocean model of the circulation in the Bay of Biscay. *Journal of Geophysical Research: Oceans*, *112*(C9), 15–33.

González-Pola, C. (2006). *Variabilidad Climática en la Región Sureste del Golfo de Vizcaya* [PhD thesis]. University of Oviedo, 192 pp.

Heezen, B. C., Tharp, M., & Ewing, M. (1959). *The floors of the oceans, 1. The North Atlantic*. Geological Society of America Special Publication, 65, 122 pp.

Hernández-Molina, F. J., Llave, E., Ercilla, G., Maestro, A., Medialdea, T., Ferrín, A., Somoza, L., Gràcia, E., Masson, D. G., García, M., Vizcaino, A., & León, R. (2008). Recent sedimentary processes in the prestige site area (Galicia Bank, NW Iberian margin) evidenced by high-resolution marine geophysical methods. *Marine Geology*, *249*(1), 21–45. https://doi.org/10.1016/j.margeo.2007.09.011

Herraiz, M., De Vicente, G., Lindo, R., Giner, J., Simón, J. L., González-Casado, J. M., Vadillo, O., Rodríguez-Pascua, M. A., Cicuéndez, J. I., Casas, A., Cabañas, L., Rincón, P., Cortés, A. L., Ramírez, M., & Lucini, M. (2000). The recent (upper Miocene to Quaternary) and present tectonic stress distributions in the Iberian Peninsula. *Tectonics*, *19*(4), 762–786. https://doi.org/10.1029/2000TC900006

Hollister, C. D., & Heezen, B. C. (1972). Geological effect of bottom currents. In A. L. Gordon (Ed.), *Studies in physical oceanography* (pp. 37–66). Gordon and Breach.

Iglesias, J., Ercilla, G., García-Gil, S., & Judd, A. G. (2010). Pockforms: An evaluation of pockmark-like seabed features on the Landes Plateau, Bay of Biscay. *Geo-Marine Letters*, *30*(3-4), 207–219. https://doi.org/10.1007/s00367-009-0182-2

Iorga, M., & Lozier, M. S. (1999). Signatures of the Mediterranean outflow from a North Atlantic climatology: 1. Salinity and density fields. *Journal of Geophysical Research: Oceans*, *104*(C11), 25985–26009. https://doi.org/10.1029/1999JC900115

Jané, G., Maestro, A., Ercilla, G., López-Martínez, J., De Andrés, J. R., Casas, D., González-Aller, D., & Catalán-Morollón, M. (2010). Occurrence of pockmarks on the Ortegal Spur continental margin, Northwestern Iberian Peninsula. *Marine and Petroleum Geology*, *27*(7), 1551–1564. https://doi.org/10.1016/j.marpetgeo.2010.04.001

Llave, E., Jané, G., Maestro, A., López-Martínez, J., Hernández-Molina, F. J., & Mink, S. (2018). Geomorphological and sedimentary processes of the glacially influenced northwestern Iberian continental margin and abyssal plains. *Geomorphology*, *312*, 60–85. https://doi.org/10.1016/j.geomorph.2018.03.022

Maestro, A., Jané, G., Fernández-Saéz, F., Llave, E., Bohoyo, F., Navas, J., Mink, S., Gómez-Ballesteros, M., Martín-Dávila, J., & Catalán, M. (2018). Echo-character of the NW Iberian continental margin and the adjacent abyssal plains. *Journal of Maps*, *14*(2), 56–67. https://doi.org/10.1080/17445647.2018.1424653

McCartney, M. S. (1992). Recirculating components to the deep boundary current of the northern North Atlantic. *Progress in Oceanography*, *29*(4), 283–383. https://doi.org/10.1016/0079-6611(92)90006-L

McCave, I. N., Hall, I. R., Antia, A. N., Chou, L., Dehairs, F., Lampitt, R. S., Thomsen, L., van Weering, T. C. E., & Wollast, R. (2001). Distribution, composition and flux of particulate material over the European margin at 47°-50°N. *Deep Sea Research Part II: Topical Studies in Oceanography*, *48*(14-15), 3107–3139. https://doi.org/10.1016/S0967-0645(01)00034-0

Olivet, J. L., Bonnin, J., Beuzart, P., & Auzende, J. M. (1984). *Cinématique de l'Atlantique nord et central*. Rapport Science et Technologie, Paris, CNEXO, 54, 5 pl., 108 pp.

Paillet, J., Arhan, M., & MacCartney, M. S. (1998). The spreading of Labrador Sea water in the eastern North Atlantic. *Journal of Geophysical Research: Oceans*, *103*(C5), 10223–10239. https://doi.org/10.1029/98JC00262

Pingree, R. D., & Le Cann, B. (1990). Structure, strength and seasonality of the slope currents in the Bay of Biscay region. *Journal of the Marine Biological Association of the United Kingdom*, *70*(4), 857–885. https://doi.org/10.1017/S0025315400059117

Pollard, S., Griffiths, C. R., Cunningham, S. A., Read, J. F., Pérez, F. F., & Ríos, A. F. (1996). Vivaldi 1991 – A study of the formation, circulation and ventilation of eastern North Atlantic central water. *Progress in Oceanography*, *37*(2), 167–192. https://doi.org/10.1016/S0079-6611(96)00008-0

Pratson, L. F., & Laine, E. P. (1989). The relative importance of gravity-induced versus current-controlled sedimentation during the Quaternary along the Mideast U.S. outer continental margin revealed by 3.5 kHz echo character. *Marine Geology*, *89*(1-2), 87–126. https://doi.org/10.1016/0025-3227(89)90029-7

Rodríguez-Fernández, L. R., López-Olmedo, F., Oliveira, J. T., Medialdea, T., Terrinha, P., Matas, J., Martín-Serrano, A., Martín Parra, L. M., Rubio, F., Marín, C., Montes, M., & Nozal, F. (2014). *Mapa Geológico de España y Portugal a escala 1:1.000.000*. Instituto Geológico y Minero de España.

Seton, M., Whittaker, J., Wessel, P., Müller, R. D., DeMets, C., Merkouriev, S., Cande, S., Gaina, C., Eagles, G., Granot, R., Stock, J., Wright, N., & Williams, S. (2014). Community infrastructure and repository for marine magnetic identifications. *Geochemistry, Geophysics, Geosystems*, *15*(4), 1629–1641. https://doi.org/10.1002/2013GC005176

Tugend, J., Manatschal, G., & Kusznir, N. J. (2015). Spatial and temporal evolution of hyperextended rift systems: Implication for the nature, kinematics, and timing of the Iberian-European plate boundary. *Geology*, *43*(1), 15–18. https://doi.org/10.1130/G36072.1

Varela, R. A., Roson, G., Herrera, J. L., Torres-Lopez, S., & Fernandez-Romero, A. (2005). A general view of the hydrographic and dynamical patterns of the Rías Baixas adjacent sea area. *Journal of Marine Systems*, *54*(1-4), 97–113. https://doi.org/10.1016/j.jmarsys.2004.07.006

Zhang, W., Hanebuth, T. J., & Stöber, U. (2016). Short-term sediment dynamics on a mesoscale contourite drift (off NW Iberia): impacts of multi-scale oceanographic processes deduced from the analysis of mooring data and numerical modelling. *Marine Geology*, *378*, 81–100. https://doi.org/10.1016/j.margeo.2015.12.006

Ziegler, P. A. (1989). Evolution of the North-Atlantic – An overview. In A. J. Tankard & H. R. Balwill (Eds.), *Extensional tectonics and stratigraphy of the North Atlantic margin* (pp. 111–129). American Association of Petroleum Geologists Memoirs, 46.